Quantum effects in ice Ih

L. Hernández de la Peña,[a] M. S. Gulam Razul, and P. G. Kusalik
Department of Chemistry, Dalhousie University, Halifax, Nova Scotia B3H 4J3, Canada

(Received 7 June 2005; accepted 8 August 2005; published online 11 October 2005)

Quantum and classical simulations are carried out on ice Ih over a range of temperatures utilizing the TIP4P water model. The rigid-body centroid molecular dynamics method employed allows for the investigation of equilibrium and dynamical properties of the quantum system. The impact of quantization on the local structure, as measured by the radial and spatial distribution functions, as well as the energy is presented. The effects of quantization on the lattice vibrations, associated with the molecular translations and librations, are also reported. Comparison of quantum and classical simulation results indicates that shifts in the average potential energy are equivalent to rising the temperature about 80 K and are therefore non-negligible. The energy shifts due to quantization and the quantum mechanical uncertainties observed in ice are smaller than the values previously reported for liquid water. Additionally, we carry out a comparative study of melting in our classical and quantum simulations and show that there are significant differences between classical and quantum ice. © *2005 American Institute of Physics*. [DOI: 10.1063/1.2049283]

I. INTRODUCTION

Classical simulations have been extensively used to study different forms of ice[1,2] including its most common form, ice Ih.[3,4] The use of empirical water models in the context of molecular dynamics simulations has allowed the computation of the static energetics as well as the determination of lattice vibrations and their comparison with neutron scattering data.[3] The later improvement of computational power and the advancement in theoretical methodologies lead to the introduction of *ab initio* quantum mechanical approaches for the study of ice[5] and other water systems. The Car–Parinello method[6] adopted in the context of the "ultrasoft" pseudopotentials[7] and gradient corrected density functional theory offered a route for the improvement in the description of the water-water interaction.[5]

However, the quantum nature of the protons is explicitly neglected in classical molecular dynamics (MD) simulations as well as in the *ab initio* molecular dynamics approach. Furthermore, it is well-known that the inclusion of the proton's uncertainty changes significantly the structural and dynamical properties of liquid water[8,9] and it is therefore expected to have some impact on the properties of ice. Garret and co-workers[10] have previously carried out equilibrium path integral Monte Carlo (PIMC) simulations on ice Ih utilizing the SPC model[11] and have found quantum ice to be less structured and to have higher energy than classical ice in agreement with expectations. This work is the only study to date to consider the impact of the protons' quantum mechanical uncertainty in the properties of ice.

Very recently, the *rigid-body* centroid molecular dynamics method[9,12] has been successfully applied to the study of liquid water.[9,13,14] This technique, which is based on the centroid molecular dynamics method (CMD) developed by Voth and co-workers,[15] allows the computation of dynamical information as well as equilibrium properties in a very efficient manner in the context of a path integral simulation. In this paper we present the results of quantum (and classical) simulations carried out on TIP4P (Ref. 16) ice Ih over the temperature range 160–235 K using the rigid-body CMD method. Quantum effects in the radial and spatial distribution function are reported, as well as the quantum energy shift and the extent of the orientational uncertainty of the molecules in the system. We also describe the quantitative impact of quantization on the translational and orientational modes of the lattice vibrations. The utility of the rigid-body CMD methodology is thereby further demonstrated.

The paper is organized as follows. Section II describes the simulation details and shows the results of the parametrization tests. Section III first presents a detailed examination of quantum effects on equilibrium and dynamical properties of ice Ih at 220 K. We then explore the temperature dependence of the quantum effects in ice from 160 to 235 K and discuss the results of quantum melting in comparison with the melting of classical ice Ih. Finally, our concluding remarks are given in Sec. IV.

II. COMPUTATIONAL METHODS

Classical simulations were carried out using standard molecular dynamics (MD) techniques and the TIP4P (Ref. 16) potential model, starting from an initial ice Ih crystal containing 360 water molecules (45 hexagonal unit cells) at the appropriate experimental densities for temperatures of 160, 185, 205, 220, and 235 K (where the densities were determined using the lattice constants given by Röttger *et al.*[17]) The disordered proton arrangement of the initial configurations was assigned using Bernal-Fowler rules[18] such that the total dipole moment of the sample was essentially zero.[19] The Ewald method[20] with conducting boundary conditions was used to evaluate the long-range electrostatic in-

[a]Present address: Chemical Physics Theory Group, Department of Chemistry, University of Toronto, Toronto, Ontario M5S 3H6, Canada.

teractions. The quantum simulations were carried out according to the rigid-body CMD methodology[9,12,14,15] where the final classical ice configuration was the starting point of the corresponding quantum calculation. The bead dynamics were controlled with a Nosé–Hoover chain[21] thermostat of length 4. The imaginary time sampling was carried out with a time step of 0.5 fs with inertia moments on each bead twice that of the real molecule. The quasi-adiabatic implementation[9] employed three imaginary steps at each classical step. In all cases (for both quantum and classical simulations), the starting lattice was allowed to relax at constant temperature and pressure for 10 ps, where zero pressure was maintained (in the x, y, and z directions) with three independent Andersen barostats.[22] After the equilibration period, the barostats were turned off for the constant temperature and density production runs. The time steps used in the classical and quantum simulations were 1 and 0.125 fs, respectively, with typical run lengths of 0.24 ns.

It is appropriate to provide a brief justification of our choice of water potential, the TIP4P model.[16] This well-characterized four-site model was chosen partly because of its computational efficiency. It has also been recently argued[23] that TIP4P-like models are superior to other simple models in reproducing the properties of ice. Finally, the reliability of the present model and methodology has been previously demonstrated[9] by their ability to reproduce the known isotopic ratios of various properties of liquid water. We have also shown[24] that the results obtained here with the TIP4P potential are not qualitatively changed if other simple water models are employed.

An extensive analysis of the parameters required for quantum simulations was carried out for our previous rigid-body CMD calculations of liquid water (see Refs. 9 and 12). Thus we can take advantage of this work and explore the parameter space in the vicinity of these previous values. The set of parameters includes the relaxation time of the Nosé–Hoover chain[21] thermostat, the bead inertia moments and imaginary time step size, the number of quantum steps per real time step, the real time step size, and the number of beads. Considering that classical simulations of liquid water and ice are technically very similar, it is reasonable to expect that, in general, the parameters used in quantum liquid simulations will be very similar to the ones required for the quantum simulation of ice (at moderate temperatures). This hypothesis was verified by a number of tests which demonstrated that the results were independent of the parameter value chosen within a reasonable range of the parameter space. Some of the key results obtained in those tests are presented below.

Due to the differences in temperature between the liquid simulations of Refs. 9 and 12 and the ice simulations of this paper, as well as the distinctive structure and dynamics in the liquid and solid phases of water, runs with five, six, and seven beads were carried out for ice Ih at 160 K. Figure 1(a) shows the oxygen-oxygen radial distribution function of H_2O ice Ih obtained from quantum simulations using five and six beads. As can be clearly seen, the functions are essentially identical (and identical to the result for $P=7$, not shown). This observation is further confirmed with the oxygen-hydrogen radial distribution functions shown in Fig. 1(b). It is important to note that Garret and co-workers[10] also found a value of $P=5$ to be sufficiently large to obtain converged results (in comparison to simulations with $P=10$). Comparison of the linear velocity time correlation functions obtained in the present quantum simulations of ice Ih at 160 K showed that the functions are identical within their statistical errors. Additional comparison with other properties confirmed that $P=5$ provided converged results. Consequently, all quantum simulations were carried out with five beads.

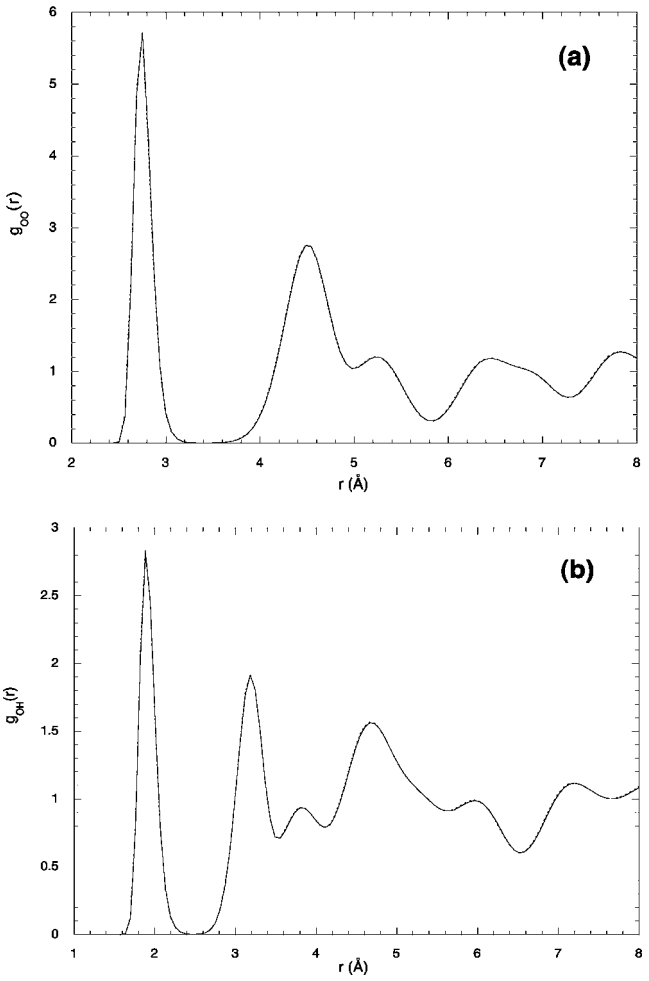

FIG. 1. Convergence of the (a) oxygen-oxygen and (b) oxygen-hydrogen radial distribution function for quantum H_2O ice Ih (at 160 K) with respect to the value of the discretization parameter P. The results represented by a dotted line and a solid line correspond to the values $P=5$ and 6, respectively.

III. RESULTS AND DISCUSSION

A. Quantum effects at 220 K

This section focuses on the results obtained in our classical and quantum simulations of ice Ih at 220 K. Our analysis will begin with the structural properties, including radial and spatial distribution functions, the energy, as well as the quantum mechanical (orientational) uncertainty; this will be followed by our discussion of the linear and angular velocity time correlation functions.

Figure 2 shows the oxygen-oxygen and oxygen-hydrogen radial distribution functions (RDFs) for ice Ih from

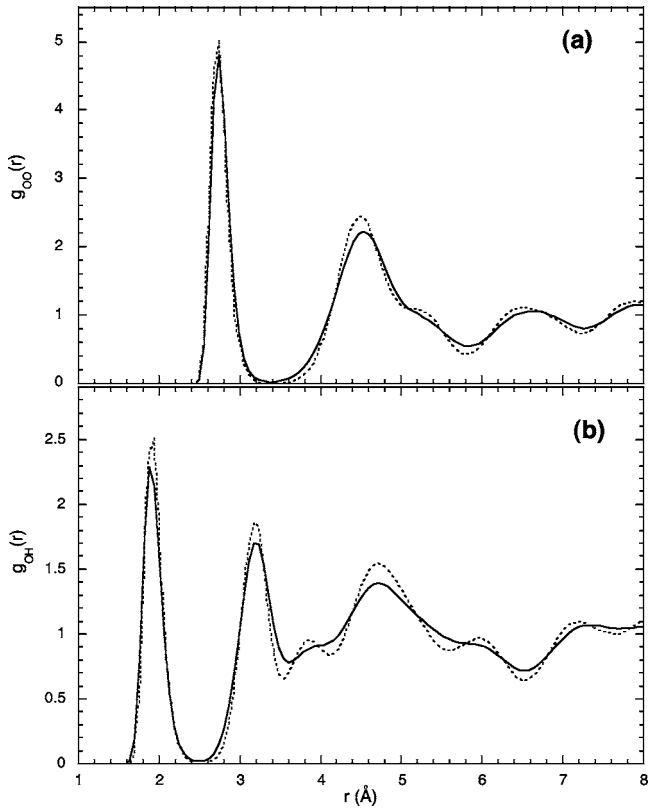

FIG. 2. Oxygen-oxygen (a) and oxygen-hydrogen (b) radial distribution functions of classical and quantum TIP4P ice Ih at 220 K. The results represented by dotted and solid lines correspond to classical and quantum simulations, respectively.

classical and quantum simulations at 220 K. The oxygen-oxygen radial distribution functions (classical and quantum) exhibit a maximum at 2.72 Å in very good agreement with the experimental[25] oxygen-oxygen distance of 2.759 ± 0.002 Å at 223 K. Both, classical and quantum simulations give very similar values for this distance. The classical results for $g_{OO}(r)$ are in good agreement with those of Vega *et al.*[26] As can be clearly seen from both Figs. 2(a) and 2(b), quantum ice exhibits decreased maxima and slightly raised minima, and can therefore be characterized as being less structured than classical ice. For example, the first peak in the oxygen-oxygen and oxygen-hydrogen RDFs is noticeably diminished by quantization. The maximum at about 4.6 Å in the oxygen-oxygen RDF, as well as the minimum at about 3.5 Å in the oxygen-hydrogen RDF, are shifted slightly outward in the quantum result compared with the classical. Taking into account the difference of scales in the plots of Fig. 2, one can conclude that the overall effect of quantization in both functions is comparable. Furthermore, since the spatial correlations in a crystalline structure extend over a much longer range than in liquid phase, the differences between classical and quantum ices are still apparent at distances of about 7 Å, in contrast to the much shorter-ranged structural effects seen in liquid water.[8,9] The results presented in Fig. 2 are qualitatively similar to the ones obtained by Garret and co-workers[10] in their PIMC simulations of ice Ih at 240 K with the SPC model. It should also be

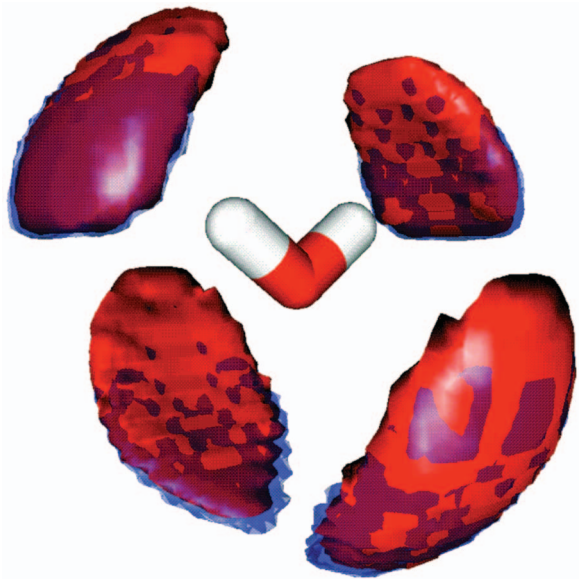

FIG. 3. (Color) Oxygen-oxygen spatial distribution function of classical (red) and quantum (semi-transparent blue) TIP4P ice Ih at 220 K. The isosurfaces correspond to $g_{OO}(\mathbf{r}_{ij})=2.8$, where only the first-neighbor features ($r_{ij}<3.5$ Å) are shown.

pointed out that agreement with the radial distribution functions obtained by Soper[27] from neutron scattering data for ice Ih at 220 K is not improved by quantization.

Figure 3 shows the oxygen-oxygen spatial distribution functions of classical and quantum TIP4P ice Ih at 220 K. The isosurfaces correspond to local oxygen densities 2.8 times that of the bulk and only the first-neighbor features (i.e., $r_{ij}<3.5$ Å) have been included for clarity. The structural manifestation of the quantum effects on the first neighbors is relatively small in comparison with those observed in liquid water.[13,14] We can see in Fig. 3 a slight shift outward of the H-bond accepting features. However, the most notable effect is in the region between the two H-bond donating features (below the central molecule) where the quantum distribution "penetrates" slightly into this relatively low probability region. This result indicates that the motion of the water molecules in the quantum lattice is slightly less restricted than in classical ice; this is in agreement with the observation (see Fig. 2) that the former is a less structured solid. The quantum effects apparent here, however, are less dramatic than in liquid water.[14]

The intermolecular potential energy of the quantum ice was found to be -47.49 ± 0.02 kJ/mol, whereas the value for the classical system was -50.84 ± 0.02 kJ/mol. This corresponds to a relative shift in the energy of 6.6%. In addition, the average orientational (or quantum mechanical) uncertainty, determined as in Refs. 9, 12, and 14, was found to be 10.2°. It is important to note that the relative energy shift and the quantum uncertainty observed in ice are smaller than the corresponding values obtained in liquid water at 298 K.[9,14] According to the results presented and discussed in Ref. 14, this is a consequence of the strong interactions between water molecules, which prevent the beads (representing the quantum degrees of freedom) from "taking advantage" of the effective weakening of the harmonic (bead-bead)

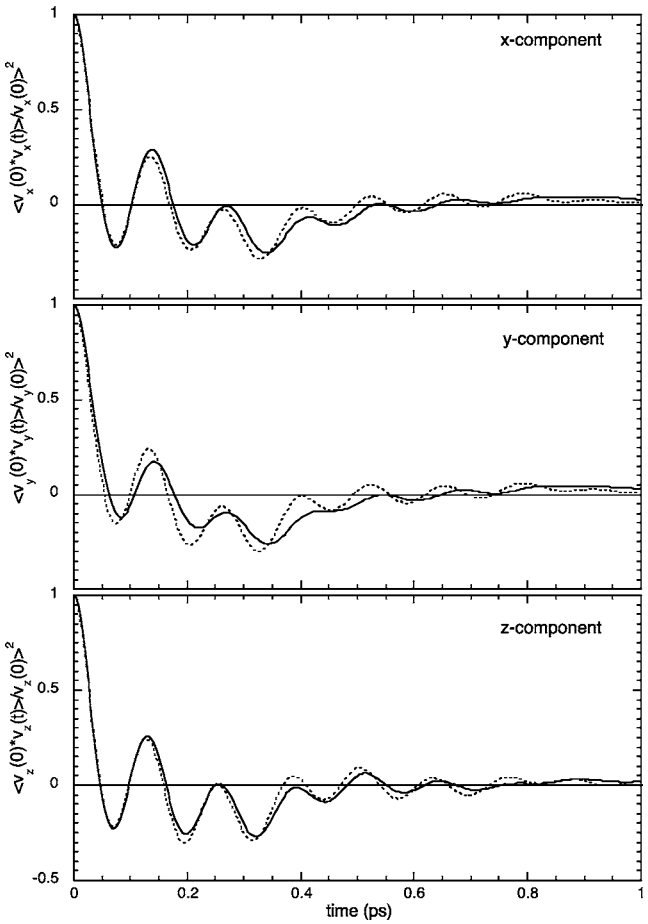

FIG. 4. Components of the linear velocity time correlation functions for classical and quantum TIP4P ice Ih at 220 K. The results represented by the dotted and solid lines correspond to classical and quantum simulations, respectively.

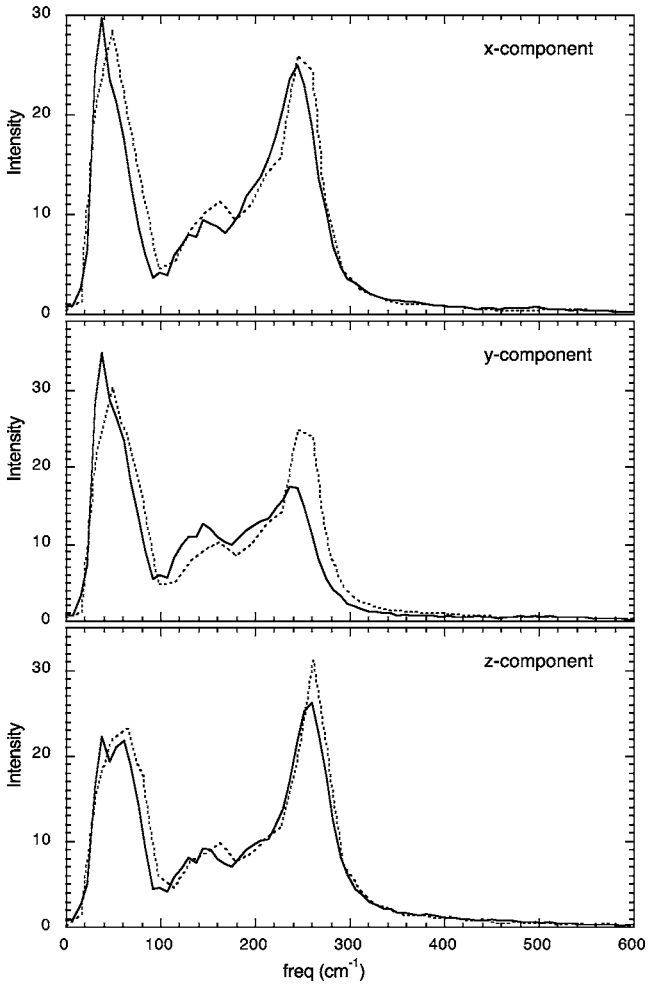

FIG. 5. Fourier transform of the components of the linear velocity time correlation functions for classical and quantum TIP4P ice Ih at 220 K. The results represented by dotted and solid lines correspond to classical and quantum simulations, respectively.

interaction[9,14] implied by a lower temperature. It should be noted that the relative shift in energy obtained from PIMC simulations with the SPC water potential at 220 K by Garret and co-workers[10] (of roughly 9%) is somewhat larger than the values determined in this work.

The present rigid-body CMD methodology allows the calculation of (approximate) quantum time correlation functions. Figure 4 shows the components of the center-of-mass linear velocity time correlation function obtained directly from classical and quantum simulations of ice Ih at 220 K. These components are defined in terms of the local frame of the molecule,[9] where the molecule lies in the *x*-*z* plane and the *z* axis is the axis of symmetry. In the quantum functions, the maxima and minima are displaced slightly toward longer times with respect to the classical functions. This behavior is particularly noticeable in the *y* component. Quantum effects are perhaps better observed in the power spectrum of these functions plotted in Fig. 5. Since these power spectra are directly related to the translational motions of the centers-of-mass, the peaks shown in Fig. 5 have been previously identified experimentally[28,29] and have also been reported in classical molecular dynamics simulations of ice Ih.[3,30] The low frequency peak corresponds to the transverse acoustic phonons, the intermediate region to the longitudinal acoustic modes, and the high frequency peak to the optic modes.[3,29] The overall shape of the spectra agrees reasonably well with experiment.[29] The effect of quantization is manifested in a rather small, but consistent, shift to lower frequencies, and appears slightly more pronounced in the *y* component. Since the *y* axis is perpendicular to the molecular plane, this result is congruent with some of the observations made in Fig. 3 regarding a more pronounced effect of quantization in the H-bond donating features of the local molecular structure. The shape of the classical and quantum spectra remains otherwise about the same.

While the linear velocity time correlation functions (Figs. 4 and 5) can be obtained directly, the angular velocity time correlation function needs to be obtained by inverse Fourier transform of $I(w)$ given by[9,15]

$$I(w) = (\hbar w/2)[\coth(\hbar w/2) + 1]C(w), \tag{1}$$

where $I(w)$ and $C(w)$ are the Fourier transforms of the quantum and centroid time correlation functions, respectively. The local frame components of the angular velocity time correlation functions were computed using Eq. (1) and are shown in Fig. 6. A dampening of the functions as well as a displacement of the maxima and minima to longer times are found. The power spectra of these functions, which primarily

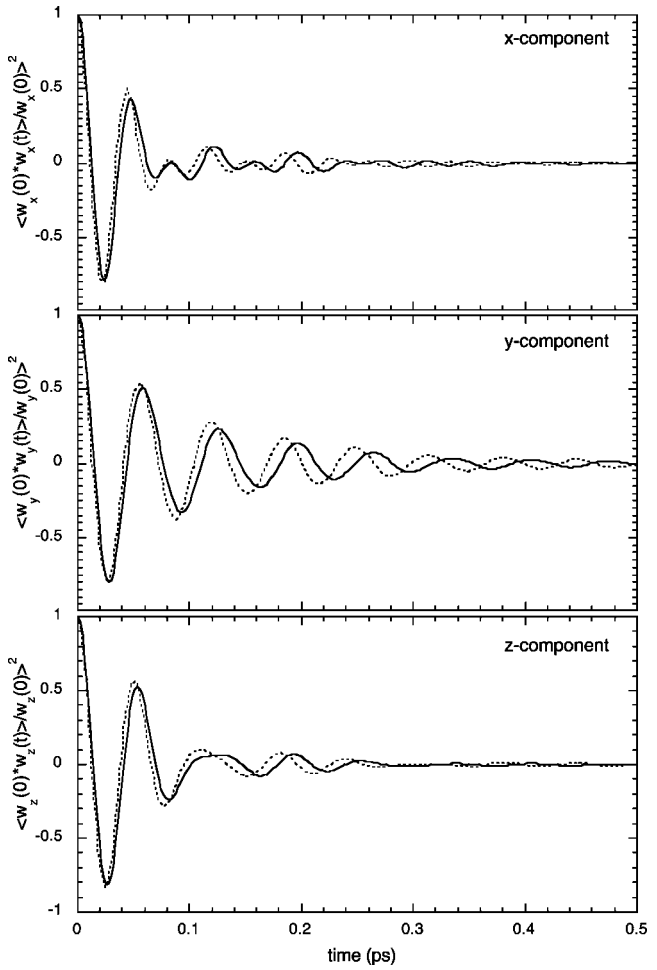

FIG. 6. Components of the angular velocity time correlation functions for classical and quantum TIP4P ice Ih at 220 K. The results represented by dotted and solid lines correspond to classical and quantum simulations, respectively.

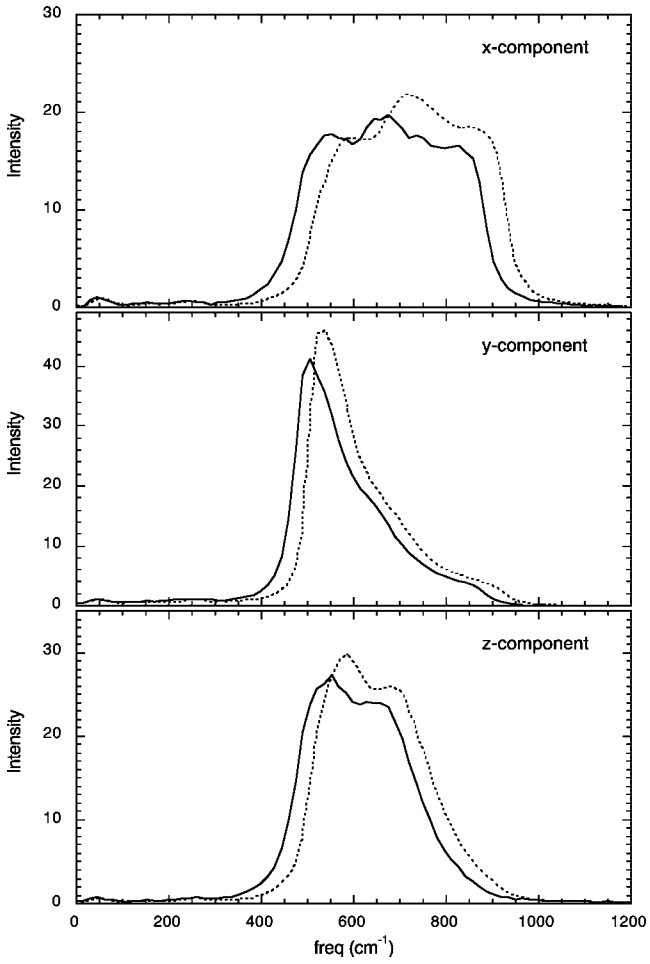

FIG. 7. Fourier transform of the components of the angular velocity time correlation functions for classical and quantum TIP4P ice Ih at 220 K. The results represented by dotted and solid lines correspond to classical and quantum simulations, respectively.

contains information about the librational motion of the water molecule in the lattice, is given in Fig. 7. The broad bands observed are indicative of the complexity of this motion. The *x* component extends to higher frequencies in comparison with the other two components as a result of having the lowest inertia moment. These librational bands have also been determined experimentally[29] and reported in previous classical molecular dynamics simulations.[3,30] The translational bands can also be seen in Fig. 7 at lower frequencies with much lower intensity, which indicates that there is some weak coupling between translational and rotational motions in ice.

The effect of quantization, a 30–50 cm^{-1} shift to lower frequencies, is much more pronounced in these rotational functions than in the power spectra of the translational motion (see Fig. 5). This is, however, expected because the orientational coordinates are directly affected by quantization. The shift, on the other hand, seems to be comparable for all three components in Fig. 7. To the best of the authors' knowledge, these shifts have not been previously reported in the literature. They can be accessed via path integral simulations, however, equilibrium path integral calculations do not contain real time dynamical information. It is in these circumstances that the concept of the centroid becomes most useful.

B. Temperature dependence of quantum effects

It is now interesting to analyze how temperature modifies the influence of quantization in ice. The general behavior expected according to quantum statistical mechanics[31] (and in particular in the path integral picture[32]) establishes that as temperature increases the quantum effects become smaller. In this section, the results from quantum and classical simulations of ice Ih carried out with the TIP4P water model over the temperature range 160–235 K are presented, where again the quantum calculations were carried out via the rigid-body CMD method (see Sec. II).

The oxygen-oxygen radial distribution functions at 160 and 235 K for classical and quantum ice Ih are presented in Fig. 8. The maximum of the first peak, at about 2.8 Å, exhibits strong temperature dependence in the classical functions as well as in the quantum results. The influence of quantization is apparent at both temperatures. While the changes in the first peak due to quantization are somewhat similar at both temperatures, the changes in the second peak, between 4 and 5 Å, are more pronounced at 235 K. Quantization, additionally, shifts these peaks slightly toward larger distances. It is important to note that, overall, the effect of

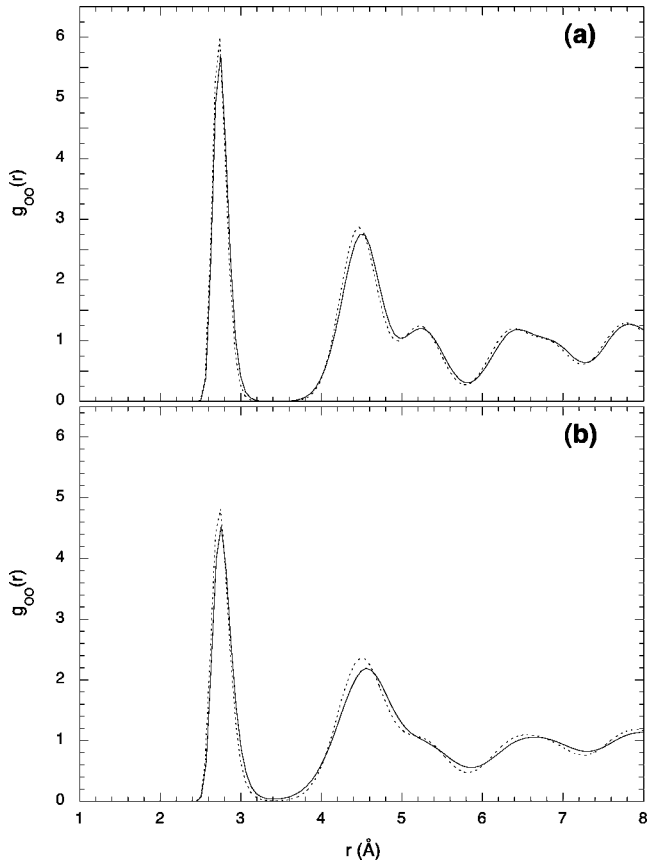

FIG. 8. Oxygen-oxygen radial distribution functions of TIP4P ice Ih at 160 K (a) and 235 K (b). The dotted and solid lines correspond to the classical and quantum, simulation results, respectively.

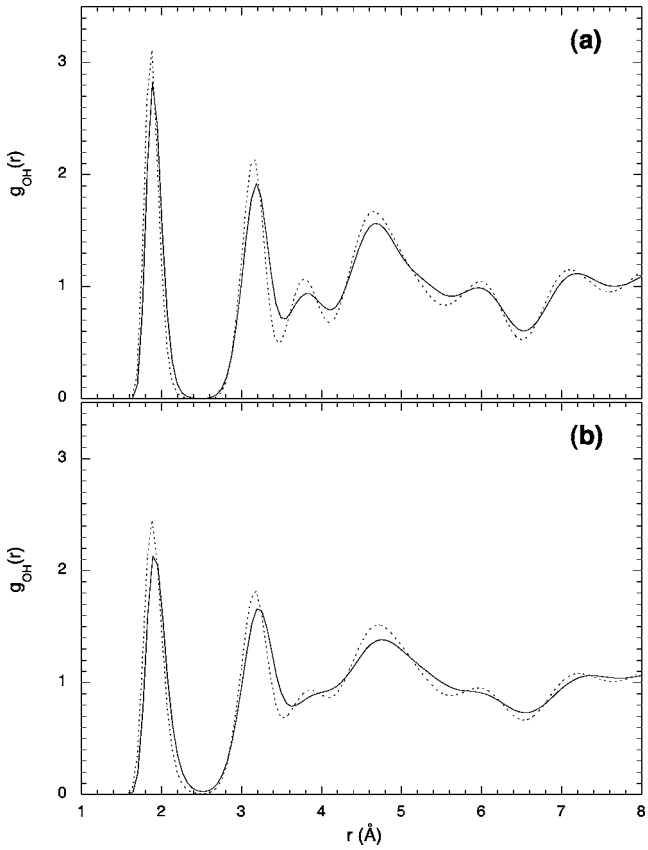

FIG. 9. Oxygen-hydrogen radial distribution functions of TIP4P ice Ih at 160 K (a) and 235 K (b). The dotted and solid lines correspond to the classical and quantum, simulation results, respectively.

the softening of the structure in this function appears more pronounced at the *higher* temperature.

Figure 9 shows the classical and quantum oxygen-hydrogen radial distribution functions of ice Ih at 160 and 235 K. Quantum effects, manifested as a softening of the functions and as a slight shift of the main features to larger distances, are apparent at both temperatures. Both effects are associated with a diminished attractive interaction in the quantum system in comparison with classical ice. The effect of "structural-softening" appears to impact specific features in Fig. 9 somewhat differently at different temperatures. For example, the third peak (between 3.4 and 4 Å), is more strongly affected by quantization at the lower temperature, however, this effect in the fourth peak (at about 4.6 Å) is more pronounced at 235 K. Consequently, the effects of quantization on these functions were judged overall to be comparable.

The results obtained for the average intermolecular potential energies (in kJ/mol) in the classical and quantum simulations of TIP4P ice Ih are plotted as a function of temperature in Fig. 10. Clearly, the intermolecular potential energy is higher in the quantum simulations than in the corresponding classical ones for all the temperatures studied. It is important to point out that, whereas the absolute shift in energies is smaller in ice than in water (see Fig. 3 of Ref. 13), described as the temperature change required to produce the same shift in energy, it is larger in ice (85 versus 60 K for liquid water[13]). The potential energy difference, quantum-classical, for ice does not increase with lower temperature as in liquid water,[13] but in fact decreases slightly, as can be seen from careful examination of Fig. 10. This is indicative of a higher heat capacity (due to intermolecular contributions) for the quantum crystal in comparison with classical ice. This could be due to the lower frequencies of the quantum lattice in comparison with the classical ice (as discussed above). This dependence of the quantum-classical energy difference

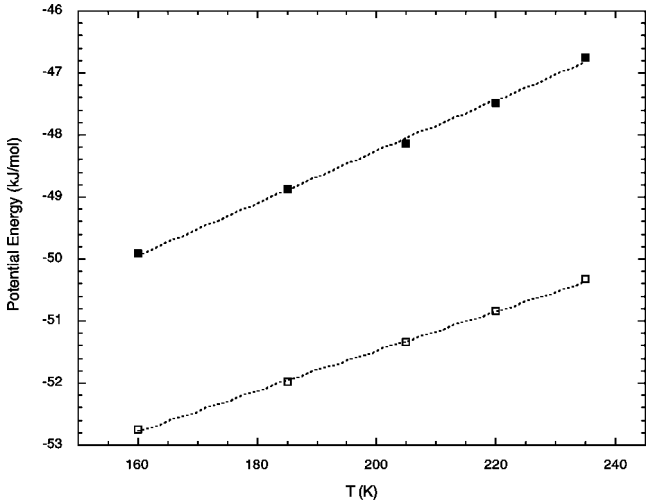

FIG. 10. Intermolecular potential energy in kJ/mol as a function of temperature. The solid squares are the results from the quantum simulations and the open squares are the classical results.

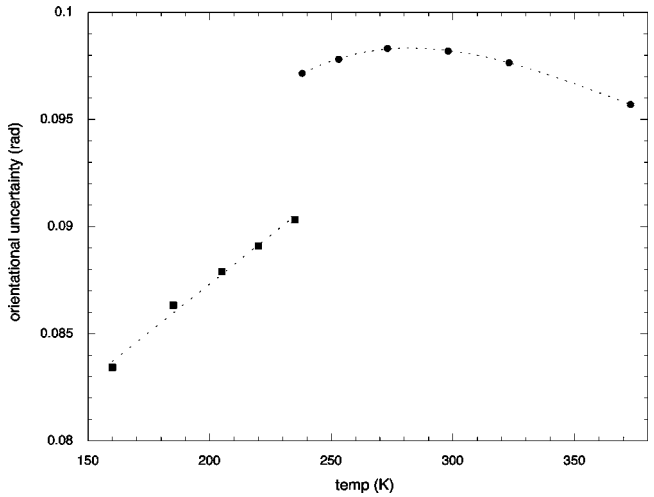

FIG. 11. Average orientational uncertainty of the water molecule in quantum ice Ih as a function of temperature (squares). The graph includes the values for liquid water (dots) from Ref. 14.

indicates that, in the temperature range studied, the largest absolute quantum effects do not occur in the lowest temperature ices, but rather within an intermediate temperature region near the solid/liquid phase boundary. This result is in disagreement with Garret and co-workers,[10] where it was found that the impact of quantum effects in the energy grew as the temperature was decreased. Moreover, at the temperatures where both phases coexist, the quantum effects in the energy are larger in the liquid phase than in ice (see also Fig. 14).

It is reasonable to expect that the trends observed for the intermolecular potential energy with temperature are, at least qualitatively, related to the quantum mechanical (or orientational) uncertainty, that is the uncertainty associated with specifying the orientation of any water molecule.[14] In Fig. 11, the average uncertainty is plotted as a function of temperature, where results obtained in quantum simulations of liquid water[13,14] have been also included. Interestingly, the orientational uncertainty in ice decreases as the temperature is lowered; this is also consistent with the previous observation that the intermolecular potential energy difference decreases with temperature. According to the discussion in Ref. 14, this behavior of decreasing molecular uncertainty when temperature is lowered is a consequence of the strength of the confining potential determined by the local molecular environment (although rather insensitive to the behavior of the density over the range of interest). It would now be interesting to determine if this dependence of the uncertainty (in liquid and solid water) is altered by a large increase in pressure, where the tetrahedral H-bonded structure of water becomes significantly distorted.

The dynamical behavior from the present ice simulations at different temperatures was also extracted and compared. From comparisons of the power spectra of the linear velocity time correlation functions of classical and quantum ice (not shown), it could be seen that the higher frequency band shifts slightly toward lower frequencies with increased temperatures. Quantization, on the other hand, also shifts the spectra toward lower frequencies, and its effect is more pronounced

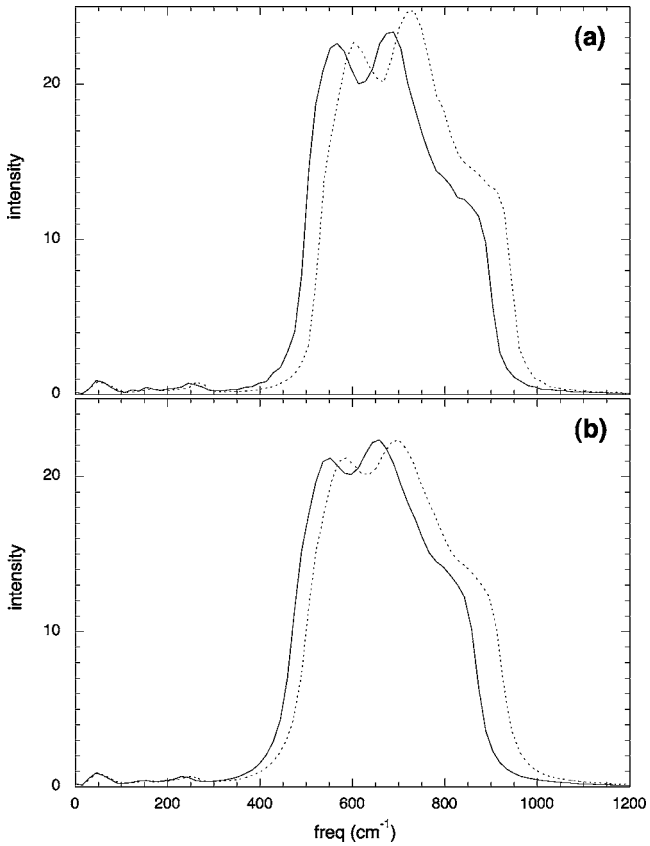

FIG. 12. Fourier transform of the angular velocity time correlation function for classical and quantum TIP4P ice Ih at (a) 160 K and (b) 235 K. The results represented by dotted and solid lines correspond to the classical and quantum simulations, respectively.

in the higher frequency bands than on the other features of the spectra for all the temperatures examined. The power spectra of the angular velocity time correlation functions of classical and quantum ice Ih at 160 and 235 K, shown in Fig. 12, reveal a consistent shift of their principal (librational) band toward lower frequencies at both temperatures. The quantum effects on these functions appear very similar at both temperatures.

C. Quantum and classical melting

We now turn our attention to the results from "computer experiments" of ice melting. The discussion here is intended to be a preliminary evaluation of the differences between the mechanical phase transition that occurs when super-heated ice Ih melts, as followed with either a classical or a quantum dynamics. It is important to emphasize that, in contrast to the use of equilibrium path integral methods (PIMC and path integral MD), the CMD approach employed in this study provides us with a clear criterion for the comparison of the classical and quantum melting processes, that is a real time variable.

Both "experiments" (classical and quantum) were carried out starting with a well-equilibrated configuration of ice Ih at 235 K. The temperature was then increased in 5 degree increments, allowing for 2 ps of equilibration and 10 ps of averaging at each step, where simulations were now carried out at a constant pressure of 1 atm. This procedure was re-

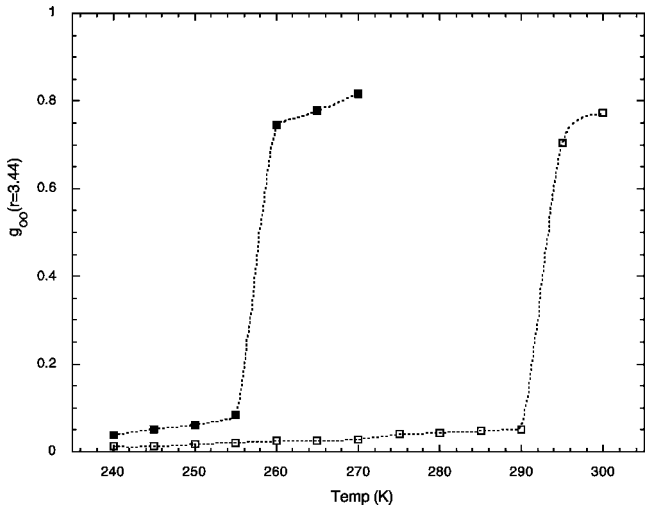

FIG. 13. Dependence of the value of the oxygen-oxygen RDF at 3.44 Å as a function of temperature for the melting of classical and quantum ice Ih. The results represented by open squares and solid squares correspond to classical and quantum simulations, respectively.

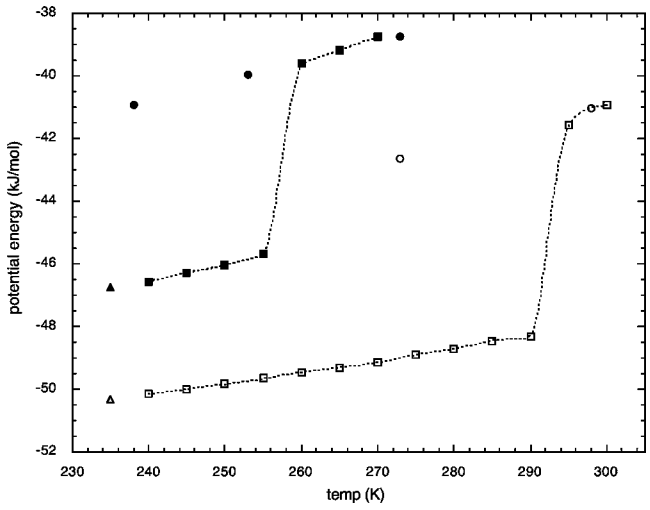

FIG. 14. Average intermolecular potential energies (in kJ/mol) as a function of temperature for the classical (open squares) and quantum (solid squares) melting of ice Ih. The graph also includes well-converged values of classical (open triangles) and quantum (solid triangles) ice at 235 K and classical (open circles) and quantum (dots) liquid water (Ref. 13).

peated until a phase transition was detected. The point immediately before the identified phase transition, as well as those after it, were subsequently re-equilibrated for a total of 40 ps and then averaged over 10 ps. This equilibration period of 40 ps allows us to establish a well-defined mechanical phase transition temperature, T_{mpt}, where super-heated ice remains crystalline over the observation time at temperatures lower than T_{mpt} and is observed to melt for temperatures at or above T_{mpt}. The thermodynamic melting temperature, T_m, is the temperature at which the bulk liquid and solid phases are in equilibrium. Thus, the melting temperature obtained in our "melting experiment" would approach T_m only with an infinite equilibration time. Therefore, these two temperatures must satisfy the relationship $T_{\mathrm{mpt}} > T_m$, which implies that any calculated value of T_{mpt} will be strongly influenced by kinetic factors. An accurate determination of the thermodynamic melting temperature would only be possible from a much more extensive simulation study, for example, of heterogeneous systems[19,33–35] or from an appropriate determination of the free energies of the bulk phases.[23,36]

Figure 13 shows the values of the oxygen-oxygen radial distribution function at 3.44 Å obtained from our series of classical and quantum simulations as a function of temperature. The near-zero value in this function for ice is reflective of the essentially zero diffusion coefficient of the crystalline phase. In liquid water, however, the oxygen-oxygen RDF has a minimum only slightly less than 1 at this distance. The radial distance 3.44 Å demarcates a reasonable limit between the first and the second coordination shells, a region that is crucially different in ice and liquid water. Indeed, the integral $4\pi\int_0^{3.44} r^2 g_{\mathrm{OO}}(r)dr$, which represents a coordination number, gives values of 4 and about 4.5 for ice and liquid water, respectively. The parameter $g_{\mathrm{OO}}(r=3.44)$ was used first by Garret and co-workers[10] in a PIMC simulation of ice Ih melting.

It can be seen from Fig. 13 that the mechanical phase transition occurs just above 290 K in the classical simulation [in good agreement with the result of a similar melting experiment conducted by McBride *et al.*,[37] but in contrast to a T_m of roughly 230 K (Refs. 23 and 36)] and just above 255 K in the quantum "experiment." This difference of about 35 K should represent an upper bound to the expected shift of the thermodynamic melting temperature. This result is in qualitative agreement with that reported by Garret and co-workers[10] for the SPC water model. They noted that quantum SPC ice Ih melts at 260 K and classical SPC ice Ih at a temperature of 280 K. Their mechanical phase transitions, however, did not appear sharp (as in Fig. 13) and lead the authors to conclude that the use of classical simulations in water for temperatures at and above 300 K is justified. However, the results shown in this work and in Refs. 8, 9, and 13 do not support this conclusion.

Figure 14 further confirms the results of Fig. 13. The former figure shows the intermolecular potential energy (in kJ/mol) obtained in the classical and quantum melting experiments as a function of temperature. Figure 14 also includes well-converged values of the intermolecular potential energy obtained for classical and quantum ice (from above), as well as classical and quantum liquid water (from Ref. 13). These latter values, which are the result of much longer simulations, serve to confirm the quality of the results obtained in the melting processes. Figure 14 also verifies that the intermolecular energy difference between classical and quantum systems is smaller in ice than in liquid water. While this observation is in agreement with the results above, it again differs from the conclusions of Garret and co-workers.[10]

IV. CONCLUDING REMARKS

In this paper, we have examined the effect of the quantum nature of the protons in the equilibrium and dynamical properties of ice Ih utilizing a rigid-body CMD approach and the TIP4P model. At 220 K, a significant softening of the structure with quantization is observed and the energy increases almost 7% in comparison with the classical results.

The average orientational uncertainty was found to be smaller than the value previously determined for liquid water at higher temperatures; this observation further verifies the importance of the local molecular environment in this property of water. The lattice vibrations associated with the librational motion experience a red shift (to lower frequencies) of about $30-50\ \mathrm{cm}^{-1}$ in relation to classical ice, whereas the shift manifested by the translational modes is much smaller.

Quantum and classical simulations were also carried out over a range of temperatures, from 160 to 235 K. The results indicate that, although quantum effects in the energy are equivalent to raising the temperature about 80 K (larger than the 60 K shift found in liquid water), the energy shifts and the average quantum mechanical uncertainties over this range of temperatures are smaller than the ones previously reported for liquid water.[13,14] The effects of quantization on the lattice vibrations associated with molecular translations and librations over this range of temperatures are also reported.

We have also employed the rigid-body CMD method to carry out a preliminary study of melting of ice Ih, where results from classical and quantum simulations were directly compared. A 35 K temperature shift due to quantization was observed to occur in the mechanical melting temperature. This result shows yet again that there are significant differences between classical and quantum ice and further demonstrates the utility of the rigid-body CMD methodology in the simulation of molecular systems in condensed phase.

Finally, it is important to note that the results presented here for the TIP4P water model are in general agreement with those obtained with other rigid water models; an extensive study of quantum liquid water and quantum ice Ih comparing several simple water models will be published in a forthcoming article.[24]

ACKNOWLEDGMENT

We are grateful for the financial support of the Natural Sciences and Engineering Research Council of Canada.

[1] A. Rahman and F. H. Stillinger, J. Chem. Phys. **57**, 4009 (1972); F. H. Stillinger, Stud. Stat. Mech. **8**, 341 (1982); O. A. Karim and A. D. Haymet, J. Chem. Phys. **89**, 6889 (1988); J. A. Hayward and A. D. Haymet, *ibid.* **89**, 6889 (1988).
[2] H. Nada and Y. Furukawa, Surf. Sci. **446**, 1 (2000).
[3] J. S. Tse, M. L. Klein, and I. R. MacDonald, J. Chem. Phys. **81**, 6124 (1984).
[4] S. C. Gay, E. J. Smith, and A. D. J. Haymet, J. Chem. Phys. **116**, 8876 (2002).
[5] C. Lee, D. Vanderbrilt, K. Laasonen, R. Car, and M. Parrinello, Phys. Rev. B **47**, 4863 (1993).
[6] R. Car and M. Parrinello, Phys. Rev. Lett. **55**, 2471 (1985).
[7] D. Vanderbilt, Phys. Rev. B **43**, 1993 (1991).
[8] R. A. Kuharski and P. J. Rossky, J. Chem. Phys. **82**, 5164 (1985); A. Wallqvist and B. J. Berne, Chem. Phys. Lett. **117**, 214 (1985); G. S. del Buono, P. J. Rossky, and J. Schnitker, J. Chem. Phys. **95**, 3728 (1991); J. Lobaugh and G. A. Voth, *ibid.* **106**, 2400 (1997); B. Guillot and Y. Guissani, *ibid.* **108**, 10162 (1998); H. A. Stern and B. J. Berne, *ibid.* **115**, 7622 (2001).
[9] L. Hernández de la Peña and P. G. Kusalik, J. Chem. Phys. **121**, 5992 (2004).
[10] H. Gai, G. K. Schenter, and B. C. Garret, J. Chem. Phys. **104**, 680 (1996).
[11] H. J. C. Berendsen, J. P. M. Postma, W. G. van Gunsteren, and J. Hermans, in *Intermolecular Forces*, edited by B. Pullman (Reidel, Dordrecht, 1981).
[12] L. Hernández de la Peña and P. G. Kusalik, Mol. Phys. **102**, 927 (2004).
[13] L. Hernández de la Peña and P. G. Kusalik, J. Am. Chem. Soc. **127**, 5246 (2005).
[14] L. Hernández de la Peña, M. S. Gulam Razul, and P. G. Kusalik, J. Phys. Chem. A **109**, 7236 (2005).
[15] J. Cao and G. A. Voth, J. Chem. Phys. **99**, 10070 (1993); **100**, 5093 (1994); **100**, 5106 (1994); J. Chem. Phys. **100**, 6157 (1994); **100**, 6168 (1994); S. Jang and G. A. Voth, *ibid.* **111**, 2357 (1999); **111**, 2371 (1999); G. A. Voth, in *Theoretical Methods in Condensed Phase Chemistry*, edited by S. D. Schwartz (Kluwer Academic, Amsterdam, 2000).
[16] W. L. Jorgensen, J. Chandrasekhar, J. D. Madura, R. W. Impey, and M. L. Klein, J. Chem. Phys. **79**, 926 (1983).
[17] K. Röttger, A. Endriss, J. Ihringer, S. Doyle, and W. F. Kuhs, Acta Crystallogr., Sect. B: Struct. Sci. **B50**, 644 (1994).
[18] P. V. Hobbs, *Ice Physics* (Clarendon, Oxford, 1974).
[19] M. S. Gulam Razul, J. Hendry, L. Hernández de la Peña, and P. G. Kusalik, Nature (to be submitted).
[20] M. P. Allen and D. J. Tildesley, *Computer Simulation of Liquids* (Clarendon, Oxford, 1989).
[21] G. J. Martyna and M. L. Klein, J. Chem. Phys. **97**, 2635 (1992).
[22] H. C. Andersen, J. Chem. Phys. **72**, 2384 (1980).
[23] C. Vega, E. Sanz, and J. L. F. Abascal, J. Chem. Phys. **122**, 114507 (2005).
[24] L. Hernández de la Peña and P. G. Kusalik, J. Phys. Chem. A (to be submitted).
[25] H. J. Prask, S. F. Trevino, J. D. Gault, and K. W. Logan, J. Chem. Phys. **56**, 3217 (1972).
[26] C. Vega, C. MacBride, E. Sanz, and J. L. F. Abascal, Phys. Chem. Chem. Phys. **7**, 1450 (2005).
[27] A. K. Soper, Chem. Phys. **258**, 121 (2000).
[28] V. F. Petrenko and R. W. Whitworth, *Physics of Ice* (Oxford University, New York, 1999).
[29] W. F. Kuhs and M. S. Lehmann, Water Sci. Rev. **2**, 1 (1986).
[30] C. J. Burnham and J. C. Li, J. Phys. Chem. B **101**, 6192 (1997).
[31] D. Chandler, *Introduction to Modern Statistical Mechanics* (Oxford University, New York, 1986).
[32] R. P. Feynman and A. R. Hibbs, *Quantum Mechanics and Path Integrals* (McGraw-Hill, New York, 1965).
[33] G.-J. Kloes, Surf. Sci. **275**, 365 (1992).
[34] L. A. Baez and P. Clancy, Mol. Phys. **86**, 385 (1992).
[35] S. C. Gay, E. J. Smith, and A. D. J. Haymet, J. Chem. Phys. **116**, 8876 (2002); T. Bryk and A. D. J. Haymet, *ibid.* **117**, 10258 (2002).
[36] E. Sanz, C. Vega, J. L. F. Abascal, and L. G. MacDowell, Phys. Rev. Lett. **92**, 255701 (2004).
[37] C. MacBride, C. Vega, E. Sanz, L. G. MacDowell, and J. L. F. Abascal, Mol. Phys. **103**, 1 (2005).